AIAA 98-2582

A Novel Investigation of the Thermoacoustic Field Inside a Rijke Tube

B. Entezam and W. K. Van Moorhem
University of Utah
Salt Lake City, UT 84112

J. Majdalani
Marquette University
Milwaukee, WI 53233

7th AIAA/ASME Joint Thermophysics and Heat Transfer Conference
June 15–18, 1998 / Albuquerque, NM

A Novel Investigation of the Thermoacoustic Field Inside a Rijke Tube

B. Entezam* and W. K. Van Moorhem†
University of Utah, Salt Lake City, UT 84112
and
J. Majdalani‡
Marquette University, Milwaukee, WI 53233

In this paper, results proceeding from experimental studies and computational simulations of the time-dependent flowfield inside a Rijke tube are presented and interpreted. A theoretical discussion based on existing speculations and scaling analyses is carried out. The main results include a similarity parameter that appears to play an important role in the heat driven oscillations. This parameter relates heat perturbations to velocity, pressure, and the square of a characteristic length. A simple theory that attributes heat oscillations to the combined effects of pressure and velocity oscillations is discussed via computational, experimental, and scaling considerations. Since previous analytical theories link heat oscillations to *either* velocity or pressure oscillations, the current analytical model agrees with and *reconciles* between existing speculations. In compliance with the Rayleigh criterion, it is found that the heat source must be positioned at a critical distance of *l*/4 from the Rijke-tube lower end for resonance to occur. This observation confirms our proposed interpretation since the critical point where coupling is maximized corresponds to a spatial location where the acoustic intensity, product of both acoustic velocities and pressures, is largest. Numerical simulations show that pressure oscillations inside the Rijke tube grow exponentially with increasing heat input. With a sufficiently small heat input, the acoustic sinks exceed the sources and acoustic damping takes place. When the heat input is augmented beyond a critical threshold, acoustic sinks become insufficient causing rapid acoustic amplification by virtue of internal energy accumulation.

Nomenclature

a_0 = mean speed of sound inside the Rijke tube
A = oscillatory pressure amplitude
A_{obs} = surface area of obstacle or heater element
C_p = constant pressure specific heat
$\bar{h}$ = heat transfer coefficient
$\bar{I}$ =acoustic intensity
l = internal tube length
m = longitudinal oscillation mode, $m = 1,2,3,...$
P =acoustic power
$p^{(1)}$ = oscillatory pressure component
Q = heat
q = heat transfer rate, dQ/dt
$q^{(1)}$ = oscillatory heat transfer rate
T = temperature
t = time
$u^{(1)}$ = oscillatory velocity component
V =volume
x = axial distance from the bottom-end
γ = mean ratio of specific heats
λ = acoustic spatial wavelength
ρ = air density
ω = circular frequency, $m\pi a_0 / l$

Subscripts
in = refers to an incoming quantity
obs = refers to the obstacle or heat source
out = refers to an outgoing quantity
∞ = surrounding mean flow condition

Superscripts
(0) = denotes a steady or mean component
(1) = denotes an unsteady/oscillatory component

*Research Scientist, Advanced Science & Technology Corp., Salt Lake City, UT. Member AIAA.

†Professor, Department of Mechanical Engineering. Senior Member AIAA.

‡Assistant Professor, Department of Mechanical and Industrial Engineering. Member AIAA.

I. Introduction

THIS investigation is carried out in an attempt to explain the heat transfer mechanisms that cause heat driven acoustic oscillations inside a classic Rijke tube configuration. It is a continuation of a previous work dedicated entirely to the numerical simulation of the flowfield inside the Rijke tube.[1] The reader is reminded that the phenomenon of heat driven acoustic oscillations belongs to the field of thermo-acoustics, which deals with interactions between heat and sound. On that account, whenever a flickering flame or heat source is enclosed in a chamber, the potential for heat-driven acoustic oscillations exists. Sometimes high intensity sound pressure levels are generated by such acoutic oscillations in systems exhibiting a likeness to Rijke or Soundhauss tubes. Naturally, such consequences may or may not be desirable depending on the type of application.

One of the applications for the thermo-acoustic system is its usage in coal-fired power plants which generate large amounts of particles. For the case of atmospheric combustors, these particles escape along with the flue gases and cause air pollution problems. Conventional removal methods are able to eliminate up to 99% of particles. These conventional methods allow over 70 percent of the number of particles (in the form of very fine particles) to escape and cause respiratory problems in the populace. Generally, particles smaller than about 5 microns are not efficiently removed. In trying to circumvent this deficieny, it has been contended that acoustic energy is capable of promoting the agglomeration of fine ash particles entrained in high temperature gas streams.[2-8] Acoustic agglomeration is a process in which high intensity sound is used to assemble micron and submicron sized particles in aerosols. The effect of sound is to cause relative motions between particles and increase their collision rate. As particles collide, they tend to bond and form larger particles. As a result, the average particle size in the aerosols increases in a short period of time. The larger particles can be more effectively separated from exhaust gases by conventional particulate removal devices. This has the beneficial effect of reducing particulate emissions and simplifying clean-up systems. Acoustic energy can also be employed to increase the rate and extent of coal combustion, allowing combustors to release larger amounts of heat.[7-8] Thermo-acoustic systems can therefore perform several beneficial functions such as: promoting higher combustion efficiency, fuel savings, reduced pollutant formation, increased fuel residence time in the combustion chamber, increased convective heat transfer rates and lower operating and equipment costs. The basic mechanisms that trigger the beneficial consequences are invariably associated with controlling the acoustic field, in order to improve mixing and/or heat transfer.

In contrast to their function in industrial applications, heat-driven oscillations in solid propellant rocket motors are undesirable. Since acoustic pressure amplitudes in excess of 10% of mean operating pressures are not uncommon in rockets, the corresponding thermo-acoustic field has been referred to as “screaming,” “screeching,” and “chugging,” which are indicative of the nature of sound produced. Clearly, resulting oscillations can cause unwanted vibrations plaguing instrumentation and payloads to the point of modifying rocket performance and throwing a missile off course.[9]

The coupling mechanism investigated in this work inside a Rijke tube may be present in a variety of problems incorporating heat, pressure and velocity perturbations, including solid and hybrid rocket motors. It is likely that the numerical code developed for this type of pulsed combustor be successfully employed in other applications as well.

For that purpose, the present analysis begins with a brief descriptions of pulse combustors, followed by a description of the self-excited oscillator that defines the character of the Rijke tube. Next, a brief dimensional analysis is addressed to reveal important group parameters that are needed to establish a condition of similitude in a Rijke tube. The test apparatus will be discussed to verify experimentally relevant observations. The computational model will be presented, followed by a discussion of experimental and numerical results. Numerical results will be shown to be in accord with existing experimental and theoretical predictions to the point of providing useful tools that tend to (1) clarify existing speculations and (2) improve existing analytical models.

II. Pulse Combustion

Pulse combustion differs from conventional combustion, where fuel is consummated under steady conditions, in being characterized by cyclical phenomena during the burning process. The cyclic or oscillatory behavior can occur spontaneously or it can be triggered by an external device such as a spark plug or an acoustic driver. Pulsating combustion is achieved spontaneously when the heat released by the combustion process occurs at one of the system’s natural frequencies. This excites acoustic pressure waves and leads to the onset of a strong coupling between acoustic energy and the combustion process. Acoustic wave interactions with the combustion process result in heat flux fluctuations. The strength of the coupling is contingent upon the magnitude of mean heat input within the system. For instance, at relatively low heat input, the coupling with the acoustic environment can be insignificant, due to small unsteady amplitudes.

On the other hand, coupling at higher acoustic oscillation modes can require appreciably higher heat input. In order for the oscillations to persist, the rate at which heat is removed from the system by way of heat transfer must not exceed the rate at which fluctuating heat energy is produced.

Pulse combustors[10] that have been developed to date can be divided into three categories according to their operational system geometry. These are the Schmidt tube (closed-open, quarter-wave system), the Helmholtz resonator (closed-open or open-open system, less than a quarter wave), and the Rijke tube (open-open, half-wave system).

A. The Rijke-Tube Concept

Among the first accounts of thermo-acoustical oscillations is that of Rijke[11] in 1859. In his work, Rijke discovered that strong oscillations occurred when a heated wire screen was placed in the lower half of an open-ended vertical pipe shown schematically in Fig. 1. Reported acoustic oscillations were found to stop altogether when the top end of the pipe was sealed, indicating that upward convective air currents in the pipe were essential for thermo-acoustically driven oscillations to take place. As could be inferred from Fig. 1, the Rijke tube is a half wave pulse combustor since the acoustic wavelength is actually twice the length of the tube. From experimental reports, oscillations reached maximum amplification when the heater was located a quarter way from the bottom.[12-15] At that location, both acoustic pressure and velocity are non-zero. For heater positions in the upper half of the pipe, damping instead of driving occurred. Rijke believed that rising convection currents expanded in the region of the heated screen and compressed downstream from the heater due to cooling at the pipe walls. Accordingly, production of sound was attributed to successive expansions and contractions. This explanation remained limited since it could not address the details of heat exchange mechanisms causing the actual oscillations.

B. The Rayleigh Criterion

Since Rijke's discovery, there has been a number of theoretical and experimental attempts to explain this phenomenon.[11-16] Lord Rayleigh[11] proposed a criterion in which he addresses the relationship between heat addition and sound waves. According to Rayleigh's criterion, energy is fed into an acoustic disturbance when heat is added to a sound wave at the high temperature phase of its cycle; conversely, energy is lost from a sound wave when heat is added at the low temperature phase. Since compression in a sound wave is adiabatic, pressure and temperature fluctuations are in phase, or

$$p^{(1)} = A \exp\left[i\left(\omega\ t - \frac{\pi}{2} \right) \right] \sin\left(\frac{n\pi}{l} x \right) \qquad (1)$$

$$T^{(1)} = \frac{A}{C_{p_0} \rho_0} \exp\left[i\left(\omega\ t - \frac{\pi}{2} \right) \right] \sin\left(\frac{n\pi}{l} x \right) \qquad (2)$$

As a result, heat addition during a positive pressure disturbance increases the amplitude of the sound waves. Clearly, an opposite effect is seen when the pressure disturbance is negative. This is similar to the effect of heat addition in thermodynamic cycles. When heat is added at the high-pressure phase of a cycle, the system gains energy. In the lower half of the Rijke tube, for instance, as the acoustic pressure approaches its maximum amplitude, the acoustic and mean velocities will both be upwards and therefore combine constructively. This enhances the local heat transfer, strengthens the coupling with the heat source, and leads to thermo-acoustic driving.

The Rayleigh's classic explanation for the Rijke tube parallels a two-cycle internal combustion (IC) engine process. The difference is that pulse combustion in an IC engine occurs at noncontant volume and is controlled by external devices. In a Rijke tube, the chamber volume remains constant and the pulsations occur naturally due to the system's internally generated harmonic waves. In the IC engine, spark plugs are fired during the moment of highest compression, usually when the piston is just past the top of its stroke, causing energy release and thermal expansion waves. Similarly, energy is removed during the moment of maximum expansion by ejection of the combustion products through exhaust valves during the low-pressure portion of the cycle. The periodic action of the spark plug, fuel injector, and exhaust valves maintain the oscillatory action of the piston and satisfy the conditions required by the Rayleigh criterion. Accordingly, the amplitude of oscillations are expected to increase when

$$\oint q^{(1)}\ p^{(1)}\ dt > 0 \qquad (3)$$

where $q^{(1)}$ is the instantaneous energy rate added to the gas flow, $p^{(1)}$ is the acoustic pressure, t is the time, and symbol $\oint$ denotes integration over one cycle of oscillation.

III. Governing Wave Equations

The wave equations with the heat addition term acting as a driving function can be written for acoustic pressure and velocity as follows:

$$\frac{1}{a_0^{\,2}}\frac{\partial^2 p^{(1)}}{\partial t^2} - \nabla^2 p^{(1)} = \frac{1}{C_p T^{(0)}}\frac{\partial q^{(1)}}{\partial t} \tag{4}$$

$$\frac{\partial^2 u^{(1)}}{\partial t^2} - a_0^{\,2}\,\nabla^2 u^{(1)} = -\frac{\gamma - 1}{\rho^{(0)}}\frac{\partial q^{(1)}}{\partial x} \tag{5}$$

Equations (4) and (5) are characteristic of self-excited or "feedback" oscillations owing to the nature of the right-hand-side terms. Since the unsteady driving force $q^{(1)}$ that appears in Eqs. (4-5) is not externally controlled, but rather induced by fluctuations in other properties within the system, the Rijke tube is of the self-excited type.

By close examination of Eqs. (4-5), the presence of three unknown variables is realized. The dependence of $q^{(1)}$ on the acoustic pressure and/or velocity must therefore be established if closure to the problem is desired. Proper auxiliary conditions in the vicinity of the heat source must also be expressed. Since no analytical formulation can ensue from Eqs. (4-5) without an additional equation that sets the model character, an appropriate relationship linking $q^{(1)}$ to $p^{(1)}$ and/or $u^{(1)}$ must precede any further theoretical speculations. Such a relationship will be explored in the present investigation. Other relationships have been proposed in the literature including the following interpretations:

A. Pressure Coupling

Chu[17] assumes that, in thermoacoustical systems, the rate of heat addition is directly proportional to the rate of pressure generated, namely that

$$\frac{q^{(1)}}{C_{p_0} T_0} = K\frac{\partial p^{(1)}}{\partial t} \tag{6}$$

which, when used in conjunction with Eq. (4), gives

$$\frac{1}{a_0^{\,2}}\frac{\partial^2 p^{(1)}}{\partial t^2} - \nabla^2 p^{(1)} = K\frac{\partial p^{(1)}}{\partial t} \tag{7}$$

This homogeneous differential equation was shown to be decaying for $K \le 0$, and growing for $K > 0$. Additionally, Chu suggested that $K = \varepsilon\left(p^{(0)^2} - p^{(1)^2}\right)$ so that

$$\frac{1}{a_0^{\,2}}\frac{\partial^2 p^{(1)}}{\partial t^2} - \nabla^2 p^{(1)} = \varepsilon\left(p^{(0)^2} - p^{(1)^2}\right)\frac{\partial p^{(1)}}{\partial t} \tag{8}$$

The last equation describes self-sustained, large-amplitude pressure oscillations which increase until reaching a steady limit-cycle oscillation. Chu's pressure coupling idea is useful to explain how heat and pressure oscillations are self-sustaining. However, it fails to explicate several important phenomena observed in the Rijke tube such as explaining the reason why no driving can occur at a velocity node despite maximum local pressure amplitudes. In addition this assumption does not satisfy the Eq. (3). This assumption may be valid for closed-open systems such as the Soundhauss singing tube[19]. Clearly, Chu's assumption does not apply to the Rijke tube.

B. Velocity Coupling

Rather than attributing the coupling of heat oscillations to internal pressure fluctuations, another proposed relationship suggests that heat and velocity oscillations are essentially behind the coupling mechanism. As such, Zinn[18] assumes that for a combustion-driven Rijke tube the heat transfer from the gauze (i.e., source) to the gas depends upon the magnitude of the total instantaneous velocity; mathematically, this translates into

$$q = C + a\left|u^{(0)} + u^{(1)}\right| = C + q^{(0)} + q^{(1)} \tag{9}$$

where C and a are constants, $u^{(0)}$ is the mean flow velocity, and $u^{(1)}$ is the acoustic velocity, and where C can be taken as zero for the case of the internal combustion process. This relationship is an improvement on the previous formulation attributing the driving source to pressure coupling. However the symmetry and coupling that exists in Eqs. (4) and (5) lead us to beleive that the heat oscillations should be a function of both acoustic pressure and velocity.

IV. Theoretical and Scaling Analysis

A. Theoretical Analysis

When heat is added to a volume of air, the air density diminishes. This causes an expansion of the volume occupied by the heated air. The periodic expansion and contraction of this volume stemming from oscillatory heat input rates produces pressure waves. These pressure waves can in turn affect the time-dependent thermal oscillations. Growing heat oscillation amplitudes are reported in the Rijke tube when the heat source is placed at a point where both acoustic pressure

and velocity have the same sign. Experimental observations also indicate that when the heat source is located at a distance of $l/4$ from the bottom, the amplitude of pressure oscillations is maximized. This point corresponds to a maximum product of pressure and velocity. In order to reconcile with existing observations, a theoretical relationship between acoustic heat, pressure, and velocity is suggested. This relationship has the form

$$q^{(1)} \propto p^{(1)}u^{(1)} \tag{10}$$

where the right-hand side, $p^{(1)}u^{(1)}$, known as the energy-flux vector modulus, represents the instantaneous energy flow per unit area for a given body of volume V. The time average of this vector is the acoustic intensity $\bar{\boldsymbol{I}}$:

$$\bar{\boldsymbol{I}} = \left\langle p^{(1)}\boldsymbol{u}^{(1)} \right\rangle = \frac{1}{t}\int_0^t p^{(1)}\boldsymbol{u}^{(1)}dt \tag{11}$$

where integration is carried out over a complete cycle. The acoustic energy $\bar{\boldsymbol{I}}$ has the dimensions of power per unit area. The integral of $\bar{\boldsymbol{I}}$ over a surface with unit normal $\boldsymbol{n}$ gives the acoustic power crossing the surface:

$$P = \int_A \left\langle p^{(1)}\boldsymbol{u}^{(1)} \bullet \boldsymbol{n}dA \right\rangle \tag{12}$$

B. Scaling Analysis

Using basic concepts from fluid mechanics, a standard dimensional analysis is attempted to establish a condition of similitude in the Rijke tube. Since computational fluid dynamics (CFD) and laboratory experimentation are both time-consuming and expensive, a practical goal here is to obtain the most information from the fewest experiments and/or computer runs. Other than the important physical insight that these similarity parameters could provide, they can be generally used for data condensation and concise presentation using the minimum number of plots.

The heat oscillation is expected to be affected by variations in several variables. The most significant ones are: the amplitude of pressure oscillation ($p^{(1)}$), amplitude of velocity oscillation ($u^{(1)}$), amplitude of temperature oscillation ($T^{(1)}$), temperature difference measured from heat source ($T_{obs} - T$), heat source location (x_{obs}), heat source diameter (d_{obs}), frequency of oscillations (f), viscosity (μ), density (ρ), specific heat (C_p), heat transfer coefficient ($h^{(1)}$), speed of sound (a_0), tube length (L), and tube diameter (D). The dependence of the dimensional heat oscillation on these parameters can be expressed as

$$q^{(1)} = f\left(p^{(1)}, u^{(1)}, T^{(1)}, T_{obs} - T, x_{obs}, d_{obs}, f, \mu, \rho, C_p, h^{(1)}, a_0, L, D\right)$$

where the form of the function f is not yet known. It is to be established from numerical considerations and later verified experimentally. After finding the rank of the dimensional matrix and applying the Buckingham-Pi Theorem, we choose $p^{(1)}, u^{(1)}, T^{(1)}$, and D as repeating parameters, and construct 11 Pi parameters. These are:

$$\pi_1 = \frac{q^{(1)}}{p^{(1)}u^{(1)}D^2};\ \pi_2 = \frac{\rho u^{(1)2}}{p^{(1)}};\ \pi_3 = \frac{C_p T^{(1)}}{u^{(1)2}};$$

$$\pi_4 = \frac{f D}{u^{(1)}};\ \pi_5 = \frac{a_0}{u^{(1)}};\ \pi_6 = \frac{h^{(1)}T^{(1)}}{p^{(1)}u^{(1)}};\ \pi_7 = \frac{\mu u^{(1)}}{p^{(1)}D};$$

$$\pi_8 = \frac{x_{obs}}{D};\ \pi_9 = \frac{L}{D};\ \pi_{10} = \frac{d_{obs}}{D};\ \text{and}\ \pi_{11} = \frac{T_{obs} - T}{T^{(1)}}$$

Since other dimensionless parameters can be formed from the original set obtained above by direct multiplication or division of a given similarity parameter or its reciprocal by another one, an alternative set can be obtained without violating the rules of dimensional analysis. Some well-identified dimensionless sets are listed in Table 1. In compliance with the Buckingham Pi theorem, the relationships to be sought are of the form:

$$\Pi_1 = F\left(\Pi_2, \Pi_3, \Pi_4, \Pi_5, \Pi_6, \Pi_7, \Pi_8, \Pi_9, \Pi_{10}, \Pi_{11}\right)$$

or

$$\frac{q^{(1)}}{p^{(1)}u^{(1)}D^2} = F\left[\frac{p - p^{(0)}}{\rho u^{(1)2}}, \frac{\rho u^{(1)2}}{\rho C_p T^{(1)}}, \frac{f L}{a_0}, \frac{u^{(1)}}{a_0}, \frac{h^{(1)}\left(T_{obs} - T\right)}{p^{(1)}u^{(1)}}, \frac{\mu \dfrac{u^{(1)}}{D}}{p^{(1)}}, \frac{x_{obs}}{L}, \frac{L}{D}, \frac{d_{obs}}{D}, \frac{T^{(1)}}{T_{obs} - T}\right]$$

or

$$q^{(1)} = p^{(1)}u^{(1)}D^2\ F\left[E_u{}^{(1)},\ E_c{}^{(1)},\ n,\ M^{(1)},\right.$$

$$\frac{h^{(1)}\left(T_{obs}-T\right)}{p^{(1)}u^{(1)}}, \frac{\mu\dfrac{u^{(1)}}{D}}{p^{(1)}}, \frac{x_{obs}}{L}, \frac{L}{D}, \frac{d_{obs}}{D}, \frac{T^{(1)}}{T_{obs}-T}\Bigg]$$

While revealing important nondimensional groupings that can be used in numerical and experimental simulations, the nondimensional analysis unveils an interesting similarity parameter relating oscillating heat flux to pressure, velocity, and characteristic length via

$$\Pi_1 = \frac{q^{(1)}}{p^{(1)}u^{(1)}D^2} \tag{13}$$

Note that Eq. (13) is in perfect agreement with the proposed formed presented in Sec. IV(A).

V. Experimental Setup

A schematic of the Rijke tube employed in the experimental part of this study is shown in Fig. 2. The experimental set-up is designed to have a simple cylindrical geometry that can be easily modified to incorporate changes when needed.

The simulated Rijke tube in this apparatus consists of several interchangeable, modular, two-inch nominal steel nipples. These interchangeable nipples are then joined together by three-way tees. The smaller side of the tee, which is perpendicular to the vertical flow direction, is connected to a short nipple, reducer, standard nipple, and a cap for inserting a microphone.

The tube is clamped in a vertical position. The total length of the tube can be changed by replacing the nipples with either shorter or longer sections. Because this is an open-open tube, the length of the tube is half the wavelength of the oscillation.

The magnitude of pressure oscillations and their frequency are measured at four different locations (through the tees) along the tube, using a Realistic microphone and a two-channel HP-3582A spectrum analyzer. To protect the microphone from the high pressure and temperature levels in the tube the microphone tip is inserted perpendicularly to the tube into the 6" long nipple rather than directly into the tube. This is done to avoid introducing vortex shedding around the microphone tip (that can interfere with measurements) and to provide a positive seal that prevents flow leakage past the microphone.

VI. The Computational Model

The two-dimensional unsteady flowfield inside the Rijke tube has been computed using FLOW-3D developed by Flow Science Corporation.[20]

In the computational model, the pipe is 90 centimeters in length and has an internal diameter of 5 centimeters. Only one cross section of the pipe is modeled, thus taking advantage of prevalent geometric symmetry (since the pipe is a body of revolution and material properties, boundary conditions and other effects are symmetric with respect to the centerline).

The computational mesh for the domain representing half of the Rijke tube and room in the x-z directions is shown by Fig. 3. A solid porous obstacle with a diameter of 3.75 cm is added inside the tube at a location of 22.5 cm from the bottom-end to model the heat source. An obstacle porosity value of 0.9 is used to represent a 90 percent open area. Thermal conductivity, density, and heat capacity of steel are used for obstacle properties. Heat is released inside the obstacle (i.e., source) as a finite time step since releasing the heat suddenly causes a numerical singularity that forces the program to crash.

A. Heat Transfer Coefficients

Quasi-steady approximations of heat transfer coefficients are evaluated automatically by FLOW-3D using standard correlations appropriate to heat convection from flat surfaces. The correlations implemented are based on four physical situations: natural convection, forced laminar convection, forced turbulent convection, and conduction within the fluid. All correlations are evaluated and the largest is used by FLOW-3D in compliance with classic heat transfer procedures.

B. Numerical Strategy

The numerical strategy consists of two stages reminiscent of transient and steady-state stages. The first stage carries the problem from an initial state of rest to a time of 20 seconds. After the first 20 seconds are elapsed, the problem reaches a terminal condition characterized by the presence of constant amplitude oscillations.

The second stage carries the problem from 20 seconds with a much smaller time interval in order to track more precisely the progressive acoustic wave growth. Virtual probes are located inside the Rijke tube model at numerous axial locations in order to monitor pressures, temperatures, densities and velocities.

VII. Results and Discussion

A. Experimental Results

The source (here using a Bunsen burner) is positioned vertically inside the lower half of the tube. The Bunsen burner heats the air around it and establishes a steady upward buoyancy driven flow in the Rijke tube. The flame is moved back and forth to locate the optimal position which excites more effectively the system's natural frequency. When this occurs, a loud and relatively pure tone is emitted and

recorder by the microphones. This loud tone is continuously produced as long as the heat flux is maintained at the source. Acoustic oscillations diminish noticeably when the outlet of the pipe is reduced or closed completely. Constricting the downstream end of the pipe produces equal and opposite (mirror) waves that reflect back and forth. This of course reduces the amplitude of acoustic oscillations. Constricting the downstream end suppresses the amount of air movement inside the tube and limits the convection heat transfer coefficient. This, of course, reduces the acoustico-thermal mode coupling. A separate test is used to verify that coupling with the naturally convected air flow is indeed a contributing mechanism to acoustic wave growth. In the verification test, a high intensity tone is emitted (indicative of acoustic wave growth) when the air flowrate is augmented externally by means of a blower located in the upper section of the pipe. Forcing the air through the tube enhances the heat transfer coefficient, leading to a stronger acoustic environment.

The same experimental verification was conducted in a Rijke tube held horizontally. Initially, using the standard procedure and configuration, oscillations did not occur. This was attributed to the absence of natural convection, which is an important contributing factor to the coupling with the acoustic waves. However, by adding a separate blower that forces air into the upper half end of the tube, a strong convective motion was induced, causing a loud tone to be generated.

Figures 4-7 show the sound pressure amplitudes (SPL) at four different locations along the pipe at the fundamental acoustic frequency. In all cases heat addition is applied approximately at the middle of the lower half (at $x = l/4$). The results presented in the above-mentioned figures are summarized in Table 2. In this case only the fundamental mode was driven at a frequency of approximately 250 Hz, which corresponds to the length of the tube (l=90 cm.). The small variations in frequency are due to the temperature fluctuations inside the tube during the test. A slight movement of the heat source either downward or upward causes the amplitude to decrease. When the heat source is moved down to the $x = l/8$ position, the second mode (f =500 Hz) appears along with the first.

B. Computational Results

Figure 8 is a graphical representation of the pressure, axial velocity, and source heat transfer versus time for the first 20 seconds. It shows that, after about 8.5 seconds, heat, pressure, and velocity oscillations begin.

Figure 9 shows the pressure, axial velocity, and source to fluid heat transfer versus time for the second stage after 20 seconds using a smaller time step to track the acoustic wave growth more accurately. This figure indicates that periodic oscillations are present in all the variables with a frequency of about 200 Hz which matches very closely the predicted natural frequency of the pipe given by $f = ma_0/(2l)$.

Figure 10 shows the pressure and axial velocity oscillations at various locations along the pipe. An examination of Fig. 10 reveals that pressure oscillations reach their maxima at the center of the pipe and minima at both ends. It also indicates that pressure oscillations are in phase at any axial location, as one would expect from acoustic wave theory. This figure also shows that velocity oscillations reach their maxima at both ends and are at a minimum at the center of the pipe. The velocity oscillations are 180° out of phase in the lower and upper half-domains.

These results exhibit the expected pattern predicted by acoustic theory, eliminating the possibility of being the mere outcome of computational error. They also agree with experimental observations in Rijke tubes.

As explained in detail in Ref. 1, it is found that a threshold for heat input intensity is required to instigate a nontrivial acoustic coupling. The phase angle between acoustic pressure and fluctuating heat flux is found to be 45 degrees. The most significant result reported previously was the verification that maximum acoustic growth occurs when the energy heat flux vector is maximum.

Figure 11 show the pressure, temperature and density distributions along the length of the tube. The numerical data provides, complete information regarding the flow properties, especially, at both ends of the heat source. Such information is necessary for setting up the boundary conditions that are needed to formulate an analytical model that allows determining $p^{(1)}$, $u^{(1)}$, or $q^{(1)}$.

The location of the source is a key factor in producing oscillations inside the Rijke tube. When the source is placed in the lower half of the pipe, large amplitude oscillations are seen to occur. The resulting oscillations are found to have the largest amplitudes when the source is located at precisely ($l/4$) from the bottom end, in agreement with experimental findings discussed previously. During separate runs, the source was relocated to the middle ($l/2$), and the upper section ($2l/3$) of the pipe in order to observe whether or not the oscillations would occur.

The numerical results indicate[1] that when the source is positioned at ($l/2$), where the amplitude of the pressure oscillation is maximum (corresponding to zero velocity), no oscillations are seen. This complies with theoretical arguments presented in Sec. IV which predict zero acoustic intensity at the chamber's mid-point. By the same token, a very weak signal is

recorded when the source is at $(2l/3)$, where the oscillatory velocity and pressure have opposite signs.

As explained in Ref. 1 the pressure oscillations inside the Rijke tube grow exponentially with increasing heat input. It appears to be a minimum value of heat addition that will allow the Rijke tube to function. With a sufficiently small heat input, the acoustic sinks exceed the sources and acoustic damping takes place. When the heat input is augmented beyond a critical threshold, acoustic sinks become insufficient and rapid acoustic amplification takes place by virtue of internal accumulation of trapped energy.

The computational work also shows that the magnitude of heat transfer oscillations is of the same order as the product of acoustic velocity amplitude, acoustic pressure amplitude, and the area of the source (see Fig. 12). This is indicative of a coupling between the acoustic heat transfer and the product of acoustic pressure and velocity in the standing wave field as predicted by dimensional analysis.

To summarize, it is observed that large oscillations occur when the product of the velocity and pressure is large at the location of the heat source. They vanish when the product is zero or negative. This seems to agree with theoretical considerations presented in Sec. IV. It appears that, at the location of the heat source, either positive or negative pressure fluctuations can be favorable in the sense of promoting acoustic wave intensification when they coincide with either positive or negative velocities. When pressure and velocity have opposite signs, oscillating fluid particles will be subjected to alternating pressure gradients that are continually unfavorable. This tends to suffocate their motion and suppress the coupling with thermal oscillations at the heat source. These conclusions drawn speculatively and confirmed numerically and experimentally seem to agree very well with the interpretation offered by Raun and co-workers regarding the effect of heat source location in a recent comprehensive review paper.[16] In congruence with our results, it is found by Raun and co-workers that "maximum driving occurs at the point a quarter of the way from the bottom of the tube where the product of the acoustic velocity and acoustic pressure has the maximum magnitude." They also agree with our result requiring both pressure and velocity fluctuations to be present for driving to occur, confirming that "driving does not occur if the gauze is placed at either a velocity or pressure node."

VIII. Conclusions

This paper complements previous work by the authors that discusses a purely numerical simulation of the flowfield inside the Rijke tube. The current investigation includes results from dimensional analysis and experimentation which are supportive of previously found results.

The dimensional analysis is useful in providing several key similarity parameters that are needed to achieve similitude in the Rijke tube. In addition to geometric scaling ratios, these include, among others, the unsteady Euler, Eckert, Mach, and acoustic mode numbers. The scaling analysis is especially useful in revealing a key parameter,

$$E_n = \frac{\overbrace{(q^{(1)} / L^2)}^{\text{Fluctuating heat flux}}}{\underbrace{p^{(1)}u^{(1)}}_{\substack{\text{Acoustic energy flux} \\ \text{vector modulus}}}}$$

consisting of the ratio of fluctuating heat flux and energy flux vector.

In addition to dimensional analysis, the experimental study discussed in this paper furnishes an independent verification of the flow character inside the Rijke tube. In compliance with previous observations, positioning of the heat source is found to be crucial for effective acoutico-thermal coupling. For example, when the heat source coincides with pressure or acoustic nodes, no acoustic amplification is observed. The same can be said when the location corresponds to acoustic velocity and pressure of opposing signs. However, when the heat source is located at one-fourth the distance from the bottom, maximum sound pressure levels are recorded. Moving away from this optimum position, which corresponds to a maximum product of acoustic pressure and velocity, a depreciation in the acoustic amplitude is noted. The experiment also indicates the importance of the air's mean flow convection currents in the coupling mechanism. It is found that unless the air's mean flowrate is appreciable, no acoustic amplification can exist. Even when generated externally via forced convection, strong air currents lead to acoustic growth.

Computational results are used to verify the role played by proper positioning of the heat source. In reiteration of previous work, it is found that (1) a minimum heat input is needed to trigger acoustic growth, (2) a 45 degree phase difference exists between acoustic pressure and fluctuating heat flux, and (3) maximum acoustic amplification occurs when the product of acoustic velocity and pressure is maximum, corresponding to a maximum energy-flux vector.

References

[1]Entezam, B., Majdalani, J., and Van Moorhem, W. K., "Modeling of a Rijke-Tube Pulse Combustor Using Computational Fluid Dynamics," AIAA Paper 97-2718, Seattle, WA, July 1997.

[2]George, W., and Reethof, G., "On the Fragility of Acoustically Agglomerated Submicron Fly Ash Particles," *Journal of Vibration, Acoustics, Stress, and Reliability in Design*, Vol. 108, July 1986, pp. 322-329.
[3]Tiwary R., and Reethof, G., "Hydrodynamic Interaction of Spherical Aerosol Particles in a High Intensity Acoustic Field," *Journal of Sound and Vibration*, Vol. 108, 1986, pp. 33-49.
[4]Reethof, G., "Acoustic Agglomeration of Power Plant Fly Ash for Environmental and Hot Gas Clean-up," *Transaction of the ASME*, Vol. 110, Oct., 1988, pp. 552-557.
[5]Song, L., Reethof, G., and Koopmann, G. H., "An Improved Simulation Model of Acoustic Agglomeration," NCA Vol. 5, 89-WA, American Society of Mechanical Engineers, Winter Annual Meeting, San Francisco, CA, Dec., 10-15, 1989.
[6]Reethof, G., Koopmann, G. H., and Dorchak, T., "Acoustic Agglomeration for Particulate Control at High Temperature and high Pressure – Some Recent results," NCA Vol. 4, 89-WA, American Society of Mechanical Engineers, Winter Annual Meeting, San Francisco, CA, Dec., 10-15, 1989.
[7]Richards , G. A., and Bedick, R. C., "Application of Acoustics in Advanced Energy Systems," NCA Vol. 3, 89-WA, American Society of Mechanical Engineers, Winter Annual Meeting, San Francisco, CA, Dec., 10-15, 1989.
[8]Yavuzkurt, S., Ha, M. Y., Reethof, G., and Koopmann, G., "Effect of Acoustic Field on the Combustion of Coal Particles in a Flat Flame Burner," *Proceedings of the 1st Annual Pittsburgh Coal Conference*, Pittsburgh, PA, Sep., 1984, pp. 53-58.
[9]Price, E. W., "Review of Combustion Instability Characteristics of Solid Propellants," *Advances in Tactical Rocket Propulsion, AGARD Conference Proceedings*, No. 1, Part 2, Chap. 5, Technivision Services, Maidenhead, England, 1968, pp. 141-194.
[10]Zinn, B.T., "State of the Art and Research Needs of Pulsating Combustion," NCA Vol. 19, 84-WA, American Society of Mechanical Engineers, 1984.
[11]Rayleigh, J.W.S., *The Theory of Sound*, Vol. 1 and 2, Dover Publications, New York, 1945, pp. 231-235.
[12]Zinn, B.T., Miller, N., Carvalho, J.A. Jr., and Daniel, B. R., "Pulsating Combustion of Coal in a Rijke Type Combustor," *Proceedings of the 19th International Symposium on Combustion*, 1982, pp. 1197-1203.
[13]Evans, R.E., and Putnam, A.A., "Rijke Tube Apparatus," *Journal of Applied Physics*, Vol. 360, 1966.
[14]Feldman, K. T., "Review of the Literature on Rijke Thermoacoustic Phenomena," *Journal of Sound and Vibration*, Vol. 7, 1968, pp. 83-89.
[15]Carvalho, J.R., Ferreira, C., Bressan, C., and Ferreira, G., "Definition of Heater Location to Drive Maximum Amplitude Acoustic Oscillations in a Rijke Tube," *Combustion and Flame*, Vol. 76, 1989, pp. 17-27.
[16]Raun, R.L., Beckstead, M. W., Finlinson, J. C. , and Brooks, K. P., "A Review of Rijke Tubes, Rijke Burners and Related Devices," *Progress in Energy and Combustion Science*, Vol. 19, 1993, pp. 313-364.
[17]Chu, B. T., "Stability of Systems Containing a Heat-Source-The Rayleigh Criterion, "NACA Research Memorandum 56D27, 1956.
[18]Zinn, B. T., Daniel, B. R., and Shesdari, T.S., "Application of Pulsating Combustion in the Burning of Solid Fuels," *Proceedings of the Symposium on Pulse Combustion Technology for Heating Applications*, Argonne National Laboratory, 1979, pp. 239-248.
[19]Feldman, K.T., "Review of the Literature on Soundhauss Thermoacoustic Phenomena," *Journal of Sound and Vibration*, Vol. 7, 1968, pp. 71-82.
[20]Flow Science Incorporated, Los Alamos, New Mexico.

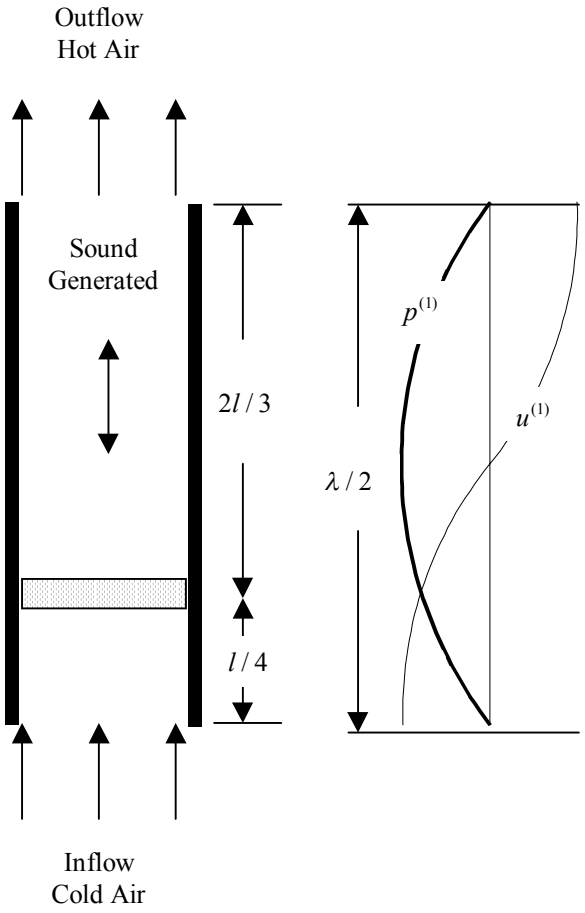

Fig. 1 The Rijke tube and associated fundamental acoustic wave structure.

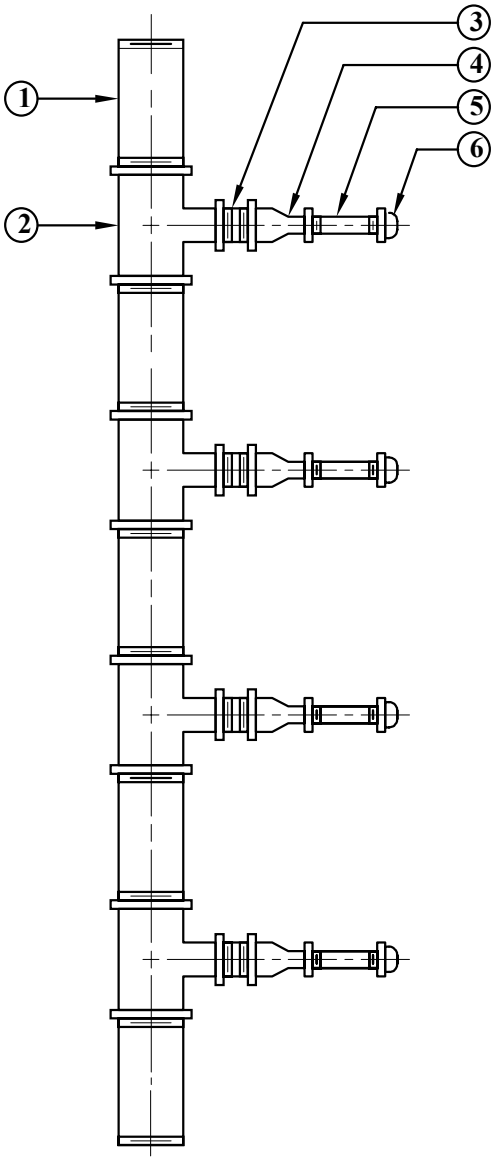

No.	Description	Size
1.	Nipple	2″ nominal
2.	Tee	2″x2″x1/2″
3.	Short Nipple	1/2″ nominal
4.	Reducer	1/2″x1/4″
5.	Nipple	1/4″x12″
6.	Cap	1/4″

Fig. 2 Schematic diagram of the experimental Rijke tube.

Table 1 The alternative dimensionless parameters for the Rijke tube

Dimensionless Parameter	Description
$\Pi_1 = \dfrac{q^{(1)}}{p^{(1)}u^{(1)}D^2}$	This is an important similarity parameter that relates the fluctuating heat flux to pressure, and velocity.
$\Pi_2 = \dfrac{p^{(1)}}{\rho u^{(1)^2}} = \dfrac{p-p^{(0)}}{\rho u^{(1)^2}}$	This is the ratio of fluctuating thermodynamic and dynamic pressures associated with the oscillating field. It is another formulation of the unsteady Euler number when written arbitrarily as $E_u{}^{(1)} = \dfrac{p^{(1)}}{\frac{1}{2}\rho u^{(1)^2}} = \dfrac{2\left(p-p^{(0)}\right)}{\rho u^{(1)^2}}$.
$\Pi_3 = \dfrac{u^{(1)^2}}{C_p T^{(1)}} = \dfrac{\rho u^{(1)^2}}{\rho C_p T^{(1)}}$	This is the ratio of the dynamic pressure and the enthalpy of the oscillating field. This parameter can also be written alternatively, by using π_{11}, as $\dfrac{u^{(1)^2}}{C_p\left(T_{obs}-T\right)} = \dfrac{\rho u^{(1)^2}}{\rho C_p\left(T_{obs}-T\right)}$. In this case, it becomes a variant formulation of the Eckert number associated with the oscillating field. By analogy to the Eckert number which, for steady flows, is defined as $E_c = \dfrac{u_\infty{}^2}{C_p\left(T_{obs}-T_\infty\right)}$, this parameter $\dfrac{u^{(1)^2}}{C_p\left(T_{obs}-T\right)} = E_c{}^{(1)}$ can be considered to be a measure of the kinetic energy of the oscillating flow per unit of boundary layer enthalpy difference referenced to the heat source enthalpy.
$\Pi_4 = fL/a_0$	This ratio is a measure of the acoustic oscillation mode number. Recalling that, for an open tube, the frequency of acoustic oscillations is given by $f = na_0/2L$, where n is the mode number, this dimensionless ratio is clearly equal to $n/2$.
$\Pi_5 = u^{(1)}/a_0$	This is the Mach number that can be associated with the oscillating flowfield.
$\Pi_6 = \dfrac{q^{(1)}}{h^{(1)}D^2\left(T_{obs}-T\right)}$	This is the ratio of the fluctuating heat flux and the unsteady convected heat associated with the fluctuating convection coefficient. According to the Newtonian cooling law, this ratio should be constant and equal to 1.
$\Pi_7 = \dfrac{\mu u^{(1)}}{p^{(1)}D} = \dfrac{\mu\frac{u^{(1)}}{D}}{p^{(1)}} \propto \dfrac{\mu\frac{du^{(1)}}{dr}}{p^{(1)}}$	This ratio scales with the ratio of shear stress and normal stress within the oscillating flowfield.
$\Pi_8 = x_{obs}/L$	This is the nondimensional spatial location of the heat source within the tube as measured from one end.
$\Pi_9 = L/D$	This is the aspect ratio of the tube.
$\Pi_{10} = d_{obs}/D$	This is the ratio of heat source and tube diameter.
$\Pi_{11} = \dfrac{T^{(1)}}{T_{obs}-T}$	This is the nondimensional temperature oscillation.

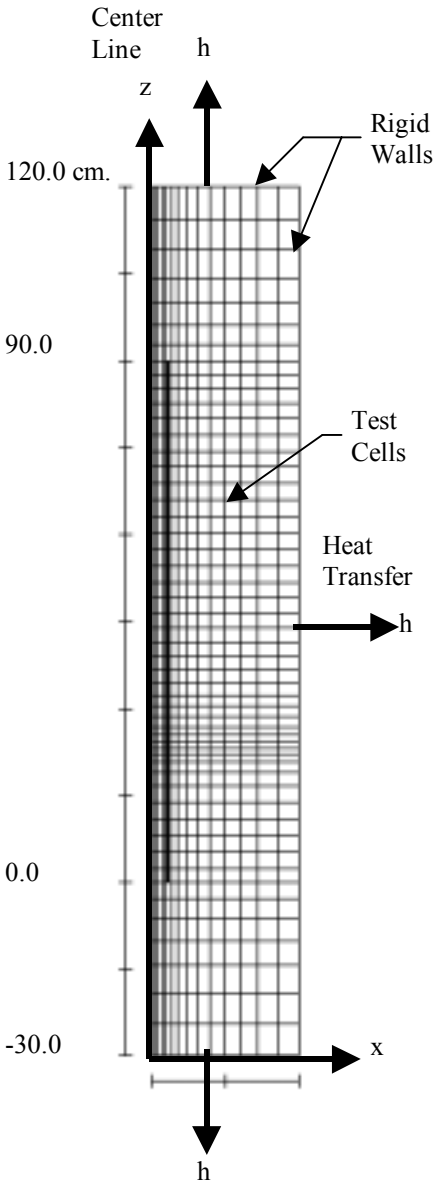

Fig. 3 Computational mesh.

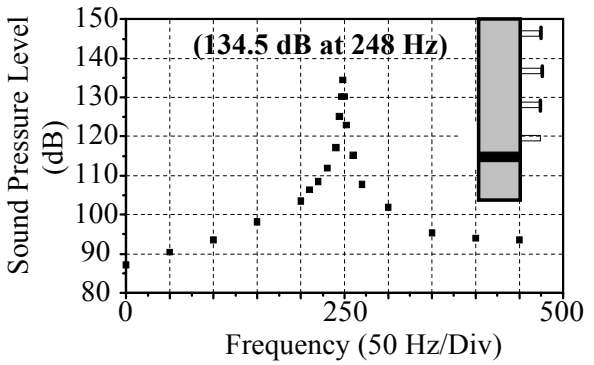

Fig. 4 Rijke Tube Oscillations. Microphone 25.0 cm. from lower end.

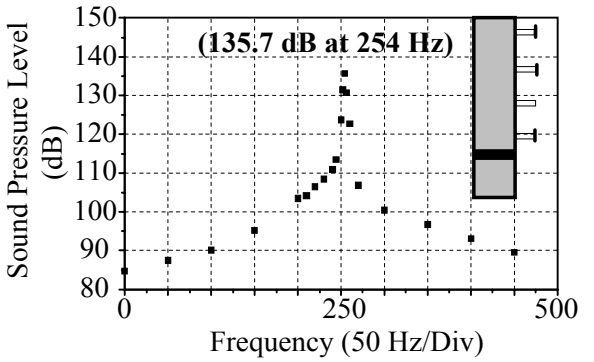

Fig. 5 Rijke Tube Oscillations. Microphone 35.0 cm. from lower end.

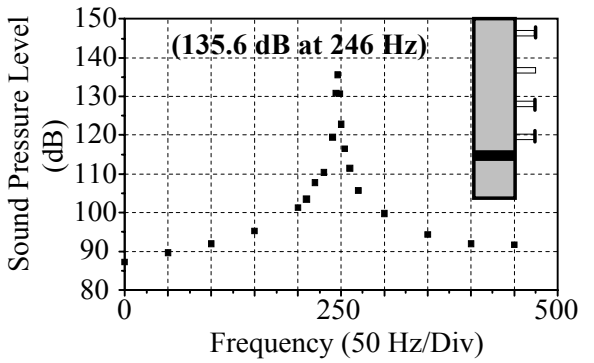

Fig. 6 Rijke Tube Oscillations. Microphone 55.0 cm. from lower end.

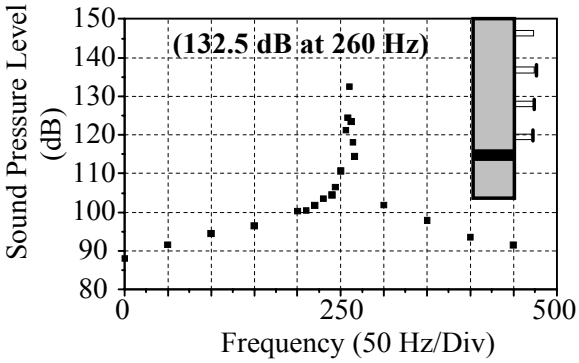

Fig. 7 Rijke Tube Oscillations. Microphone 65.0 cm. from lower end.

Table 2. Pressure amplitude at different locations along the Rijke tube

Microphone (Distance from bottom-cm)	SPL (dB)	Prms (Pa)	Frequency (Hz)
25	134.5	108.3	248
35	135.7	124.3	254
55	135.6	122.9	246
65	132.5	86.0	260

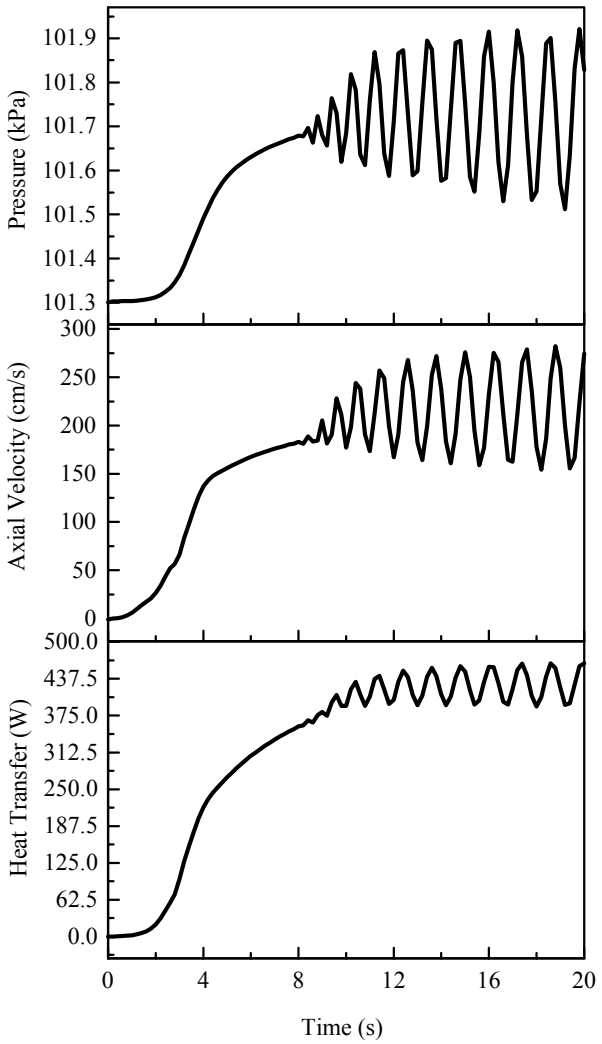

Fig. 8 Time-dependent pressure, axial velocity and heat transfer versus time during the first 20.0 seconds (Stage I). This is a standard run with 430 watts at the heater location which coincides with the virtual probe at $l/4$.

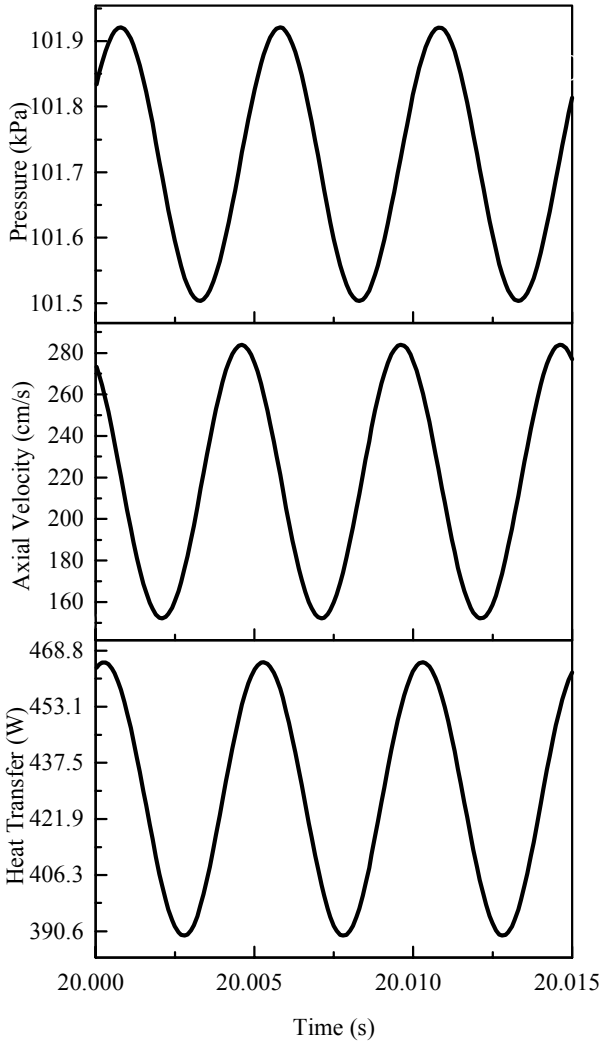

Fig. 9 Time-dependent pressure, axial velocity and heat transfer versus time for a time step of 0.0025 seconds during limit-cycle oscillations (Stage II). This is a standard run with 430 watts at the heater location which coincides with the virtual probe at $l/4$.

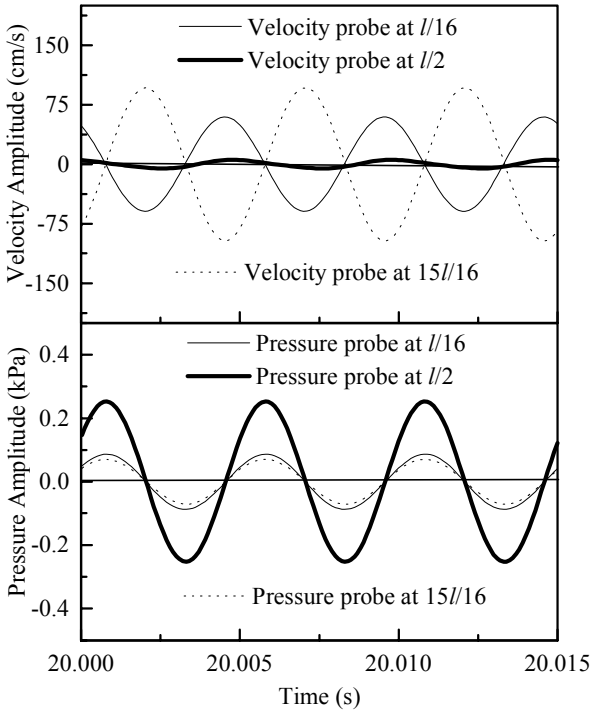

Fig. 10 Axial velocity and pressure oscillations at various locations along the pipe versus time (Stage II).

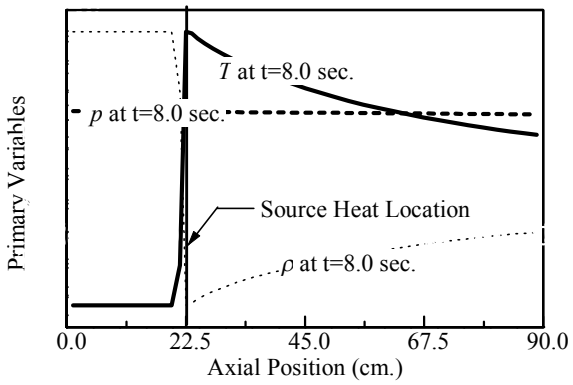

Fig. 11 Steady pressure, temperature and density at various times before the onset of oscillations (Stage I).

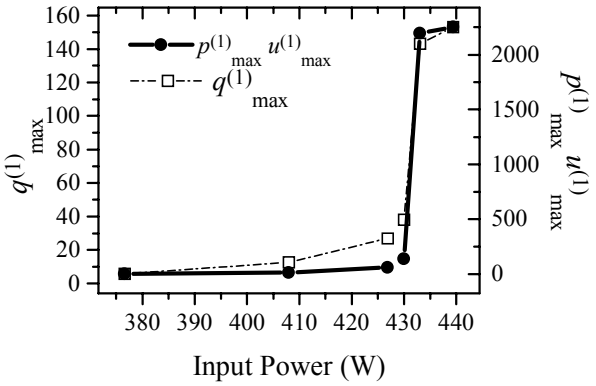

Fig. 12 Comparison between magnitude product of acoustic pressure and velocity; and heat oscillation.